# Steady-state availability of sodium channels

## Interactions between activation and slow inactivation

Peter C. Ruben, John G. Starkus, and Martin D. Rayner*

Békésy Laboratory of Neurobiology, Pacific Biomedical Research Center, and *the Department of Physiology, John A. Burns School of Medicine, University of Hawaii, Honolulu, Hawaii 96822 USA

ABSTRACT Changes in holding potential $(V_h)$, affect both gating charge (the $Q(V_h)$ curve) and peak ionic current (the $F(V_h)$ curve) seen at positive test potentials. Careful comparison of the $Q(V_h)$ and $F(V_h)$ distributions indicates that these curves are similar, having two slopes ($\sim 2.5e$ for $V_h$ from $-115$ to $-90$ mV and $\sim 4e$ for $V_h$ from $-90$ to $-65$ mV) and very negative midpoints ($\sim -86$ mV). Thus, gating charge movement and channel availability appear closely coupled under fully-equilibrated conditions.

The time course by which channels approach equilibration was explored using depolarizing prepulses of increasing duration. The high slope component seen in the $F(V_h)$ and $Q(V_h)$ curves is not evident following short depolarizing prepulses in which the prepulse duration approximately corresponds to the settling time for fast inactivation. Increasing the prepulse duration to 10 ms or longer reveals the high slope, and left-shifts the midpoint to more negative voltages, towards the $F(V_h)$ and $Q(V_h)$ distributions. These results indicate that a separate slow-moving voltage sensor affects the channels at prepulse durations > 10 ms.

Charge movement and channel availability remain closely coupled as equilibrium is approached using depolarizing pulses of increasing durations. Both measures are 50% complete by 50 ms at a prepulse potential of $-70$ mV, with proportionately faster onset rates when the prepulse potential is more depolarized.

By contrast, charge movement and channel availability dissociate during recovery from prolonged depolarizations. Recovery of gating charge is considerably faster than recovery of sodium ionic current after equilibration at depolarized potentials. Recovery of gating charge at $-140$ mV, is 65% complete within $\sim 100$ ms, whereas <30% of ionic current has recovered by this time. Thus, charge movement and channel availability appear to be uncoupled during recovery, although both rates remain voltage sensitive. These data suggest that channels remain inactivated due to a separate process operating in parallel with the fast gating charge.

We demonstrate that this behavior can be simulated by a model in which the fast charge movement associated with channel activation is electrostatically-coupled to a separate slow voltage sensor responsible for the slow inactivation of channel conductance.

## INTRODUCTION

In steady state, the fraction of sodium channels available to respond to a depolarizing voltage step is governed by the initial membrane potential. Two processes have been identified which appear to contribute to this effect of holding (or resting) potential on channel availability. First, as noted by Hodgkin and Huxley (1952), fast inactivation (which reaches steady state within $\sim 15$ ms in squid axons) limits channel availability as a function of initial potential. The $h_\infty$ curve characterizes the effects of short (2–15 ms) prepulses on sodium channel availability. Second, more slowly-equilibrating slow inactivation processes have been found in all membranes where appropriate experiments have been conducted. Narahashi (1964) found that slow inactivation of sodium current occurred in lobster giant axons during longer depolarizations than were used by Hodgkin and Huxley. Slow inactivation was subsequently described in squid axons (Adelman and Palti, 1969; Chandler and Meves, 1970d; Rudy, 1978), in *Myxicola* (Schauf et al., 1976;

Rudy, 1981), myelinated nerve fibers (Brismar, 1977), and mammalian skeletal muscle (Simoncini and Stühmer, 1987; Ruff et al., 1987). Finally, it should be emphasized that fast and slow inactivation are separate processes mediated by pharmacologically distinct mechanisms. For example, pronase (Rudy, 1978) and N-bromoacetamide (Heggeness and Starkus, 1986) and papain (Quandt, 1987) remove fast inactivation without affecting slow inactivation, whereas trypsin differentially affects slow inactivation (Starkus and Shrager, 1978).

Slow inactivation has been described in terms of an additional "$s$-gate" with its voltage-sensitivity defined by the fraction of channels available for opening following long (usually >50 ms) prepulses (Rudy, 1978; Starkus and Shrager, 1978; Quandt, 1987). Previous studies (e.g., Starkus and Shrager, 1978; Heggeness and Starkus, 1986; Ruff et al., 1987) have noted that the midpoint of the "$s_\infty$" curve is more negative than the midpoint of the "$h_\infty$" curve; this left shift in midpoint indicates an additional reduction in the steady-state availability of channels from slowly-equilibrating processes. However,

---

Address correspondence to Dr. Ruben.

comparative evaluations of steady-state availability have been complicated by the wide range of prepulse durations used in different studies (10 ms to 2 min) which may, or may not, have been sufficient to permit full equilibration of the inactivation mechanisms.

Additionally, fast inactivation processes lead to immobilization of gating charge, i.e., the temporary restraint of gating charges in their depolarization-favored positions. Fast immobilization (of gating charge) and fast inactivation (of sodium current) have identical kinetics, are similarly affected by pronase (Armstrong and Bezanilla, 1977; Bezanilla and Armstrong, 1977), and thus appear to be alternative views of a single process. On the other hand, recovery of gating current after prolonged depolarization is substantially faster than recovery of peak ionic current (Bezanilla et al., 1982; Rayner and Starkus, 1989). If the slow recovery rates for charge movement and ionic current are different, then the question may be raised as to whether their onset rates and equilibria are also different.

Both Bezanilla et al. (1982) and Rayner and Starkus (1989) concluded that the steady-state distribution of gating charge could be well described as resulting from electrostatic coupling between the activation mechanism and voltage-insensitive fast and slow inactivation/immobilization processes. Our present results extend the previous work by including effects of changing initial conditions on both peak sodium currents and gating currents. Our data indicate that slow inactivation is controlled by a separate, slow-moving, voltage sensor which is coupled, presumably through electrostatic interactions, to the activation voltage sensor(s). The additional slow inactivation voltage sensor must be included into the previous model to fully describe the control of channel availability under equilibrium (resting) conditions.

These results have been presented in preliminary form (Ruben and Starkus, 1991).

## METHODS

Medial giant axons from the crayfish, *Procambarus clarkii*, were internally perfused and voltage clamped using methods adapted to crayfish axons by Shrager (1974) and further described by Starkus and Shrager (1978). Temperature was maintained at $7° \pm 0.5°C$ throughout the experiments in this study. Series resistance was initially compensated at 10 $\Omega$-cm² and was recompensated, when necessary, to maintain constant peak amplitude of the capacity transient recorded during test hyperpolarizing steps (Alicata et al., 1989). Corrections were made for an initial electrode junction potential of 8–10 mV. Electrode drift over the course of an experiment was never greater than 1–2 mV.

Our methods for data recording and for subtraction of linear capacity and leakage currents using the $P/n$ control pulse protocols have been presented in detail by Rayner and Starkus (1989) and Ruben et al. (1990). However, particular care is required, when using either signal averaging or $P/n$ capacity subtraction protocols during experiments involving prolonged prepulses or changes in holding potential, so as to avoid progressive changes in steady-state inactivation. A typical capacity subtraction protocol, in which test pulses for signal averaging are alternated with $P/n$ control pulses from subtraction holding potential (SHP), can induce progressive recovery (where the SHP is negative), whereas the test pulse depolarizations can themselves induce an accumulating component of "use-dependent" slow inactivation. The keys to avoiding cumulative errors from signal averaging are: (a) to use appropriately long interpulse intervals, and (b) to group the test (P) and $P/n$ control pulses separately (to avoid recovery at SHP). All experiments were therefore carefully monitored using an analog storage oscilloscope (Tektronix) in parallel with our digital recording equipment. Interpulse intervals were adjusted to ensure constant signal height in any group of records taken for signal averaging.

Holding and prepulse potentials were randomized to further reduce the possibility of cumulative effects from ultra-slow inactivation (see e.g., Rudy, 1978) over the course of an experiment. Additionally, control steps (usually from −120 mV holding potential to +20 mV) were inserted between every one to three test pulses from different holding potentials (depending on axon stability) to ensure accurate rundown correction. Change in peak control currents was used to proportionately correct the intervening test currents for any indicated rundown, even when it was as small as 10% over the course of an experiment. The current records from at least four test pulses were averaged for each ionic current data point. Gating current data points were comprised of averaged currents from 8 to 16 test pulses. Leak "pedestals" were removed before integration of gating current records by zeroing the current traces over the last 0.5 ms of the 4 ms data trace.

## Solutions

Outward currents were used in this study to avoid the possibility of invasion artifacts from unclamped regions outside the control of the guard electrodes. Sodium concentrations (see Table 1) were chosen to maintain peak sodium current at <1.5 mA/cm² (while minimizing both linear and nonlinear leakage currents) by mixing high-Na and Na-free solutions in appropriate concentrations. Internal sodium was replaced by cesium on an equimolar basis where reduction of current magnitude was needed. Sodium concentrations are listed in figure

TABLE 1 **Experimental solutions**

| Condition | Na⁺ | Ca⁺⁺ | Mg⁺⁺ | Cs⁺ | Cl⁻ | F⁻ | TMA⁺ | Glutamate⁻ | Hepes | pH |
|---|---|---|---|---|---|---|---|---|---|---|
| 200 Na Internal | 200 | 0 | 0 | 30 | 0 | 60 | 0 | 170 | 1 | 7.35 |
| 0 Na Internal | 0 | 0 | 0 | 230 | 0 | 60 | 0 | 170 | 1 | 7.35 |
| 210 Na External | 210 | 13.5 | 2.6 | 0 | 242.2 | 0 | 0 | 0 | 2 | 7.55 |
| 0 Na External | 0 | 13.5 | 2.6 | 0 | 242.2 | 0 | 210 | 0 | 2 | 7.55 |

Osmolarity: 430–440 mOsm

legends as external//internal Na (in mM). Sodium was replaced with tetramethylammonium (TMA) on an equimolar basis in those experiments where gating currents were recorded. Additional junction potentials introduced by changing solutions differed from the control solution by no more than ±2 mV. Tetrodotoxin (TTX) was not used in these experiments, because Heggeness and Starkus (1986) have demonstrated that TTX reduces gating charge movement at holding potentials less negative than −120 mV, by left-shifting the curve describing gating charge as a function of holding potential.

## Computer simulations

Simulations were carried out using a Sun 3/60 computer (Sun Microsystems, Mountain View, CA). Our modeling program uses simple Euler integration to solve the array of simultaneous equations representing the allowed transitions within each particular model formulation. Cumulative errors were <0.001% at the end of each model run. All voltage steps were presumed to be instantaneous. Initial state occupancies were calculated separately for each holding potential. Multi-pulse protocols were simulated by using final state occupancies for pulse 1 as the initial state occupancy for state 2, et cetera. All transitions were specified in accordance with Eyring rate theory (Glasstone et al., 1941; Woodbury, 1971; Stimers et al., 1985). All data points were obtained by analyzing simulated records of ionic and gating currents by the same methods as used in analysis of axon data.

## RESULTS

### Effects of changes in holding potential on steady-state channel availability

When pulses to a constant test potential are used to evaluate the effect of holding potential $(V_h)$ on the fraction of open sodium channels $(F)$, the resulting $F(V_h)$ curve reflects the steady-state availability of channels. As a descriptor, $F(V_h)$ is neutral as to the underlying mechanisms. It simply defines observations based on an experimental protocol in which holding potential is fully equilibrated before the depolarizing test pulse. By contrast, the more commonly used term, "$s_\infty$", implies a direct measurement of the properties of a hypothetical "$s$-gate" without specifying the experimental methods used. Because fast inactivation may also be involved in determining the steady-state availability of channels for activation, we use here the more neutral but experimentally descriptive term $(F(V_h))$.

We evaluated steady-state channel availability by comparing $I_{Na}$ and gating charge as functions of holding potential. Holding potentials were maintained for at least 2 min before evoking ionic or gating current with a depolarizing voltage step. The order of holding potentials was randomized and rundown was carefully evaluated with appropriate corrections made when necessary (see Methods).

Fig. 1 shows that $I_{Na}$ (Fig. 1 $A$) and gating charge (Fig. 1 $B$) are suppressed to an equivalent extent at similar holding potentials $(V_h)$. These data indicate that ionic current and gating charge are associated in steady-state conditions, because both the peak $I_{Na}$ and $Q_{ON}$ are equally affected by changes in $V_h$. Fig. 1 $A$ also shows that the time-to-peak of the ionic currents are similar across the full range of holding potentials (Cole-Moore type delays are <10% of time to peak in sodium channels of crayfish axons, see Starkus and Rayner,
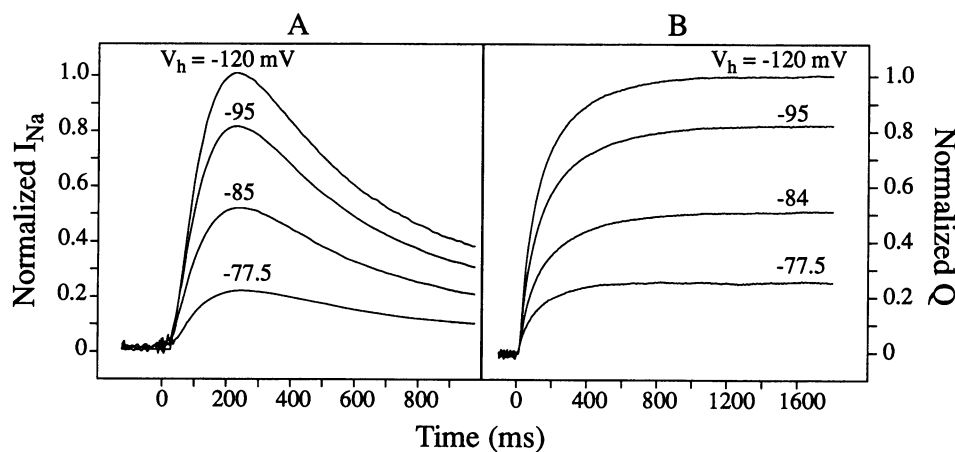


FIGURE 1 Ionic current and gating charge are similarly affected by changes in holding potential $(V_h)$. ($A$) Sodium currents are normalized to the peak current amplitude when $V_h$ was −120 mV; $I_{Namax} = 1.05$ mA/cm². ($B$) Gating currents were integrated and normalized to maximum gating charge found at $V_h$ from −110 to −140 mV; $QON_{max} = 29$ nC/cm². The $V_h$ noted above each trace equally affects both $I_{Na}$ and $QON$. Test potential was +20 mV in all cases. Ionic current and gating charge waveforms were checked for kinetic identity throughout all $V_h$. Normalization to currents at $V_h = -120$ mV was used because both the $F(V_h)$ and $Q(V_h)$ curves are flat at voltages more hyperpolarized than −110 mV. All data from axon 900628. Ionic currents recorded in 0//25 Na. Gating currents recorded in 0//0 Na, 200 TMA.

1991). This observation suggests that there was no significant series resistance error in these measurements. Similarly, in Fig. 1 B, the integration waveforms are superimposable (after rescaling) at all holding potentials. Both these criteria were carefully checked in all our experiments involving changes in holding potential.

## $F(V_h)$ distribution shows two regions of differing slope

Fig. 2 shows that steady-state channel availability does not conform to a single Boltzmann distribution. The data shown in Fig. 2 were generated by a depolarizing step to +20 mV from different holding potentials (Fig. 2 A, inset). When normalized to the maximum peak current value (from a holding potential of −140 mV), the data are roughly fit by a Boltzmann distribution with a midpoint of −90 mV. However, as seen in Fig. 2 B, the data show two distinct regions of different slope when plotted as the logit transformation. The slope (derived by least squares analysis) is $2.83e$ between $V_h$ equals −110 mV and −90 mV, and $4.69e$ between $V_h$ equals −90 mV and −70 mV.

This result was confirmed in a series of 10 experiments (see Table 2). In each experiment, slopes were determined over two ranges of holding potentials. From −115 to −90 mV, the mean slope was $2.68e$ (±0.20 SEM). For holding potentials from −90 to −70 mV, the mean slope was $4.82e$ (±0.21 SEM). These slopes differ significantly by one-way analysis of variance ($p < 0.0001$). However, the lower slope is similar to the $1.79e$ (±0.15 SD) found by Rayner and Starkus (1989) for a series of six $Q(V_h)$ curves over the same range of holding potentials (−130

to −90 mV). We noted that the $Q(V_h)$ data in Rayner and Starkus (1989) had relatively few points in the range of holding potentials between −90 and −60 mV. Therefore, we attempted to determine whether a second steeper slope would be found in that voltage range from a more rigorous study of the $Q(V_h)$ curve.

## $Q(V_h)$ distribution also shows two regions of differing slope

Gating currents were recorded from crayfish axons after sodium currents had been blocked by replacing external and internal cations with TMA. TMA does not significantly affect the waveform of gating currents in crayfish giant axons (Heggeness and Starkus, 1986) and it avoids the TTX-induced ~10 mV left-shift of $Q(V_h)$ midpoint noted in that study. Under these conditions, ON-gating currents ($Ig_{ON}$) were recorded during a depolarizing step from different holding potentials. Holding potentials were maintained for 2 min before collecting the gating current records. Gating currents were analysed by integrating for 2 ms to determine the quantity of charge that moved as a function of holding potential. Fig. 3 shows the $Q(V_h)$ curve obtained by steps to +20 mV from different holding potentials. The data were normalized to the maximum charge movement (Fig. 3 A, estimated as an average of values between $V_h$ −120 and −140 mV) and then plotted after logit transformation (Fig. 3 B). Two distinct slopes can be detected; in six axons, the average slope was $2.65e$ (±0.22 SEM) for holding potentials from −110 to −90 mV, and $3.78e$ (±0.30 SEM) for holding potentials from −90 to −65 mV (see Table 2). These slopes are significantly different, as
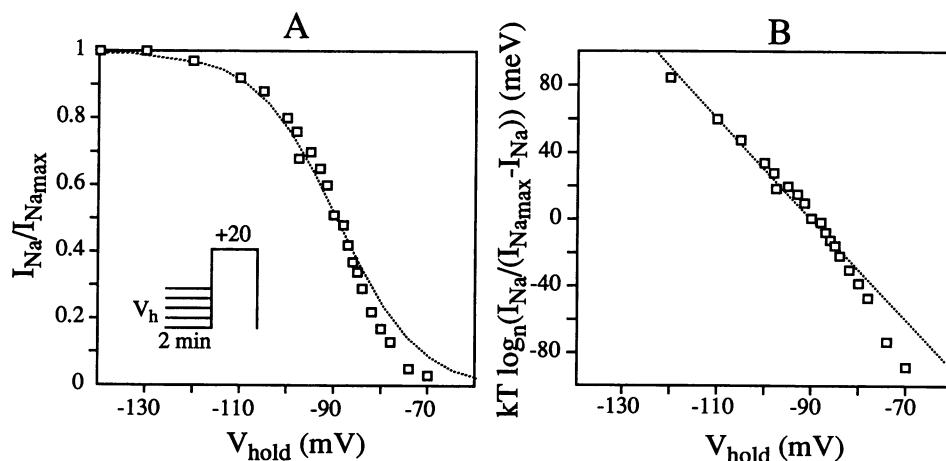


FIGURE 2  Suppression of $I_{Na}$ differentially increases at more depolarized $V_h$. (A) Currents are plotted as normalized to their averaged maximum value (from −130 to −160 mV holding potential) and plotted as an $F(V_h)$ distribution. (B) The $F(V_h)$ distribution is linearized by the logit transformation and shows two linear regions with different slopes. The dashed lines in A and B are single Boltzmann distributions with a slope of $2.8e$ and −90 mV midpoint. Data from axon 880719. (0//25 Na).

TABLE 2 $F(V_h)$ and $Q(V_h)$ slopes and midpoints

| | Experiment | Midpont (mV) | Low slope Range | Low slope Slope | High slope Range | High slope Slope |
|---|---|---|---|---|---|---|
| $F(V_h)$ | 880527 | −92 | −115 to −95 | 2.44 | −90 to −70 | 3.82 |
| | 880621 | −95 | −115 to −100 | 2.18 | −90 to −80 | 4.49 |
| | 880622 | −95 | −115 to −95 | 3.10 | −95 to −70 | 4.26 |
| | 880630 | −90 | −105 to −90 | 2.00 | −90 to −65 | 4.98 |
| | 880708 | −85 | −110 to −85 | 2.45 | −85 to −70 | 5.91 |
| | 880711 | −88 | −115 to −88 | 1.93 | −88 to −75 | 5.25 |
| | 880712 | −90 | −110 to −90 | 3.55 | −90 to −70 | 5.11 |
| | 880719 | −90 | −110 to −90 | 2.83 | −90 to −70 | 4.69 |
| | 900622 | −90 | −110 to −90 | 2.78 | −90 to −75 | 4.31 |
| | 900628 | −85 | −110 to −85 | 3.55 | −85 to −72.5 | 5.39 |
| Mean (SEM) | | −90 (±1.2) | | 2.68 (±.20) | | 4.82 (±.21) |
| $Q(V_h)$ | 900622 | −86 | −100 to −90 | 3.19 | −90 to −75 | 4.68 |
| | 900628 | −84 | −102 to −90 | 2.73 | −90 to −72.5 | 4.11 |
| | 910415 | −85 | −100 to −85 | 3.17 | −85 to −72 | 3.90 |
| | 910419B | −77 | −100 to −84 | 2.66 | −86 to −72 | 3.98 |
| | 910430B | −70 | −100 to −75 | 2.18 | −75 to −65 | 2.83 |
| | 910502 | −79 | −100 to −85 | 1.96 | −85 to −70 | 3.16 |
| Mean (SEM) | | −80.2 (±2.7) | | 2.65 (±.22) | | 3.78 (±.30) |

tested by analysis of variance ($p < .0005$). The voltage at which the two slopes diverged varied between different experiments, from 2 to 10 mV more negative than the distribution midpoint. Thus, we routinely used the voltage 5 mV more negative than the midpoint as the dividing point for statistical determinations of the separate slopes.

Fig. 4 shows that $Q(V_h)$ data and $F(V_h)$ data from one axon nearly overlie each other. Sodium currents were recorded from different holding potentials in this axon and then were blocked to record gating currents by replacing TMA for internal sodium and cesium ions. The open triangles in Fig. 4 show the ionic current and the closed triangles show the gating charge as a function of holding potential. Both are plotted as logit transformations of the normalized data. The slope of the $Q(V_h)$ curve between −102 mV and −90 mV is 2.73$e$, and between −90 and −72.5 mV is 4.11$e$. The $F(V_h)$ curve has a slope of 3.55$e$ between $V_h$ equals −110 and −85 mV, and 5.39$e$ between $V_h$ equals −90 and −75 mV. The
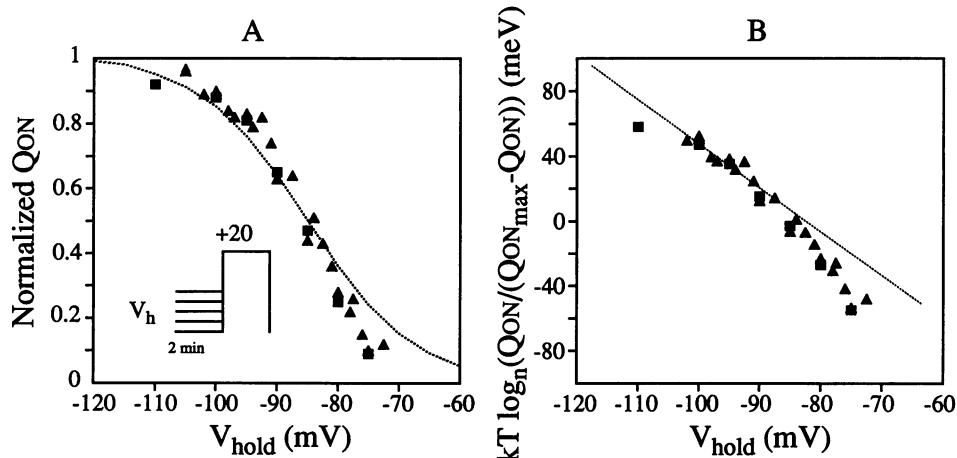


FIGURE 3 Suppression of gating charge as a function of holding potential. Gating currents were recorded in a step to +20 mV and integrated to obtain gating charge. (A) Gating charge is normalized to the averaged values obtained at holding potentials between −110 mV and −130 mV. (B) The data are plotted as the logit transformation of the normalized data. Two distinct regions with different slopes can be detected (see text). In both panels, the lines are Boltzmann distributions calculated with a slope of 2.7$e$ and a midpoint of −85 mV. Data from axons 900622 (squares) and 900628 (triangles). 200//200 TMA.
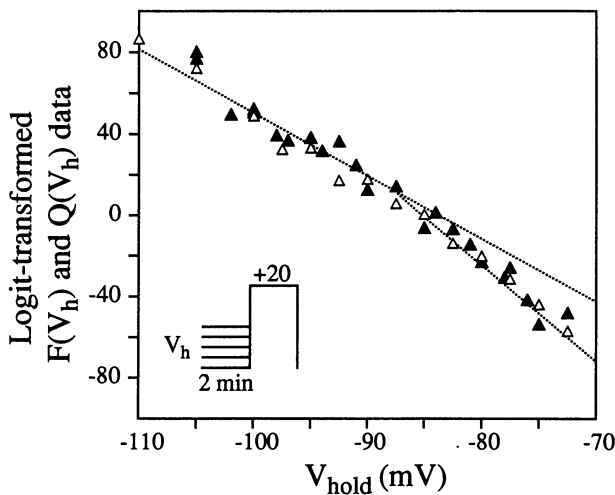
FIGURE 4  $F(V_h)$ and $Q(V_h)$ curves have similar properties. Ionic current (*open triangles*) and gating charge (*solid triangles*) data were normalized and are here plotted as the logit transform. All data from axon 900628. Lines were fit to the data by least squares linear regression to the low (3.14*e*) and high slope (4.75*e*) regions of the $Q(V_h)$ data. Ionic currents were recorded in 0//25 Na. Gating currents were recorded in 200//200 TMA.

similarity between the voltage dependences of charge movement and peak ionic current suggests that these processes are closely related under these experimental conditions.

Despite the close correspondence between $F(V_h)$ and $Q(V_h)$ data noted above, the mean data from Table 2 suggests a 10 mV difference in the midpoints for these distributions. However, similar midpoints were measured in the two experiments (900622 and 900628) in which both $F(V_h)$ and $Q(V_h)$ data were obtained from the same axons. These two experiments (and the earlier gating current experiments) used TMA in the internal perfusate. However, the earlier ionic current experiments used a cesium internal perfusate, rather than TMA, which might explain the slight shift in midpoint in those experiments. Thus, the apparent difference in $Q(V_h)$ and $F(V_h)$ distribution midpoints indicated in Table 2 was not supported by additional experiments (such as that shown in Fig. 4) in which both distributions were determined in the same axons.

## Time course of equilibration during depolarizing prepulses

The data of Table 2 demonstrate a 30 to 40 mV left-shifting of the $F(V_h)$ and $Q(V_h)$ midpoints relative to the midpoint of the $Q(V)$ distribution in crayfish axons ($-50$ mV, Rayner and Starkus, 1989) and a 60 to 70 mV

left-shift by comparison with the $-20$ mV midpoint of the $F(V)$ distribution (Ruben et al., 1990). We have therefore explored the relative contributions of fast and slow inactivation in this marked left-shifting of the steady-state availability curves in crayfish axons.

In most axons, fast inactivation is followed by a clear plateau of steady-state sodium current (Chandler and Meves, 1970*a–c*; Oxford and Yeh, 1985). The maximum time required to reach this plateau current, at negative test potentials, defines the minimum prepulse duration required to characterize the $h_\infty$ curve. In crayfish axons (see Starkus and Rayner, 1991) this plateau is less obvious and the "steady-state" $I_{Na}$ decays, with time constants $> 100$ ms, to very small levels at all test potentials. Nevertheless, an apparent break between fast and slow falling phase kinetics occurs within about 2 ms in our axons even at near threshold potentials. We have therefore used a 2 ms prepulse as the minimum prepulse duration for the $h_\infty$ curves shown here.

### Increasing prepulse durations shift the $h_\infty$ curve to the left

Fig. 5 demonstrates that the midpoint of the $h_\infty$ curve shifts to the left with increase in prepulse duration. The midpoint of the curve showing $I_{Na}$ as a function of a 2-ms prepulse potential (*open squares*) is $-49$ mV and overlies the curve showing gating charge as a function of a 2-ms prepulse potential (*solid squares*). With a 10-ms prepulse (*crosses*), the $I_{Na}$ curve has a midpoint of $-65$ mV. When the prepulse duration was 100 ms (*gray squares*), the midpoint of the distribution is $-77$ mV. These values approach the midpoints for the $F(V_h)$ and $Q(V_h)$ distributions ($-85$ mV, *open triangles* and $-84$ mV *solid triangles*, respectively), obtained following 2 min at each holding potential.

### Increasing prepulse duration adds a high slope region to the $h_\infty$ curve

Fig. 5 also shows that two slopes are clearly visible in data recorded using prepulses of 10 ms (*crosses*) and longer. For 100-ms prepulses, the slopes are 1.10*e* in the low slope region (correlation coefficient $r = 0.89$) and 3.52*e* in the high slope region ($r = 0.99$). On the other hand, only a single slope is visible in both ionic current and gating charge data recorded using a 2-ms prepulse (*open and solid squares*). In this case, the slope of the ionic data is 1.73*e* across the voltage range over which data was recorded ($r = 0.98$). The gating current data has a slope of 2.25*e* across the entire voltage range ($r = 0.93$).
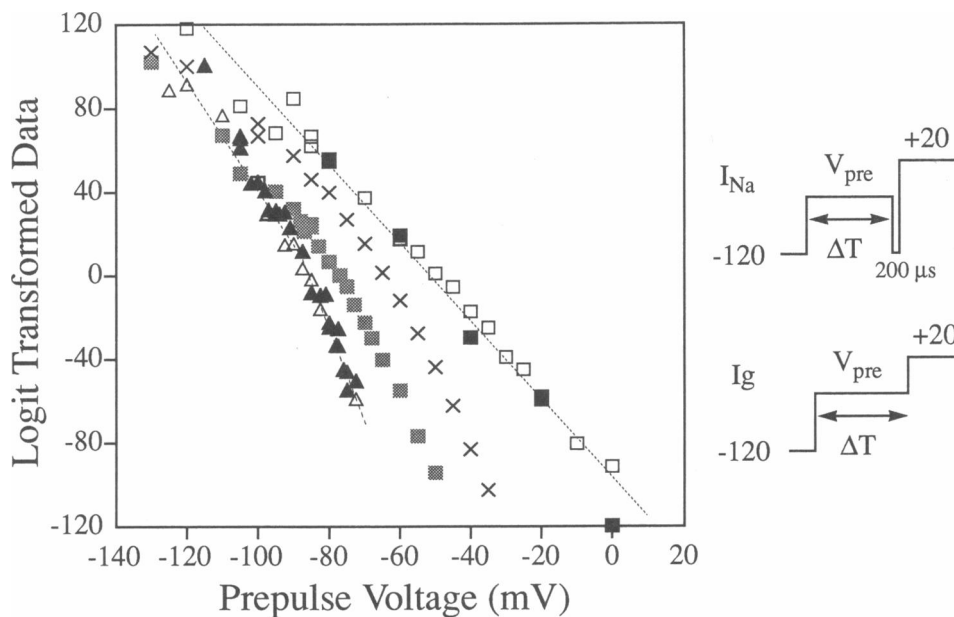
FIGURE 5  Voltage sensitivity is altered by increasing prepulse durations. Ionic currents (*open symbols*) and gating charge (*solid symbols*) are plotted as logit transformed data. Gating charge (as a function of prepulse potential) following a 2 ms prepulse (*solid squares*) overlies the $I_{Na}$ curve for a 2-ms prepulse (*open squares*). The steady-state charge distribution (*solid triangles*) also overlies the $F(V_h)$ curve (*open triangles*). Other symbols show distributions for different prepulse durations (*crosses* = 10 ms; *grey squares* = 100 ms). Lines are fit to the data by least squares. Ionic current data from axons 880726 (2- and 100-ms prepulse), 880728 (10-ms prepulse) and 900628 (steady state). Gating current data from axons 870626 and 870624 (2-ms prepulse) and 900628 (steady state).

## Kinetic analysis of channel equilibration during depolarizing and hyperpolarizing prepulses

### Onset

The kinetics of the equilibration processes were studied by applying depolarizing prepulses of increasing duration and measuring, in the same axons, the peak sodium current or gating charge movement during the subsequent test pulse. Fig. 6 shows for short (*A*) and longer (*B*) prepulse durations that both peak ionic current and gating charge movement are suppressed with similar kinetics. This observation was confirmed for two prepulse voltages. The onset rates are markedly voltage sensitive; onset was faster at −40 mV prepulse potentials (*squares*) than with −70 mV prepulses (*triangles*). The voltage dependence of both onset measures, as well as their kinetics, are similar; both develop to approximately the same fraction of control amplitudes for a given prepulse potential. Taken together, these results suggest that channel availability and gating charge movement are effectively coupled during depolarizing prepulses.

Fig. 7 demonstrates that onset and recovery rates of test pulse $I_{Na}$ are similar when assessed at the same

prepulse potential. In both cases, the prepulse potential to induce (*squares*) or remove (*triangles*) slow inactivation was −90 mV (see pulse inset). Fig. 7 more clearly shows the duration of prepulses required to approach complete slow inactivation of sodium current. To directly compare onset and recovery rates, the data for onset were inverted. The line is a double exponential, fit by the methods of least squares and has a fast time constant of 600 ms and a slow time constant of 2 s. These data indicate that slow inactivation of test pulse $I_{Na}$ conforms to the properties expected of a Markovian system, because both onset and removal of slow inactivation have the same rates at the same prepulse potential.

### Recovery

In contrast to their onset, test pulse ionic current and gating charge movement do not recover at the same rates. Fig. 8 shows ionic currents (*A*) and gating charge (*B*) across the same range of prepulse durations. Current and charge amplitudes have been normalized to the maximum (fully recovered) values. For each prepulse duration, gating charge shows greater recovery than ionic current although recovery rates apparently approach each other at longer times (>300 ms). For
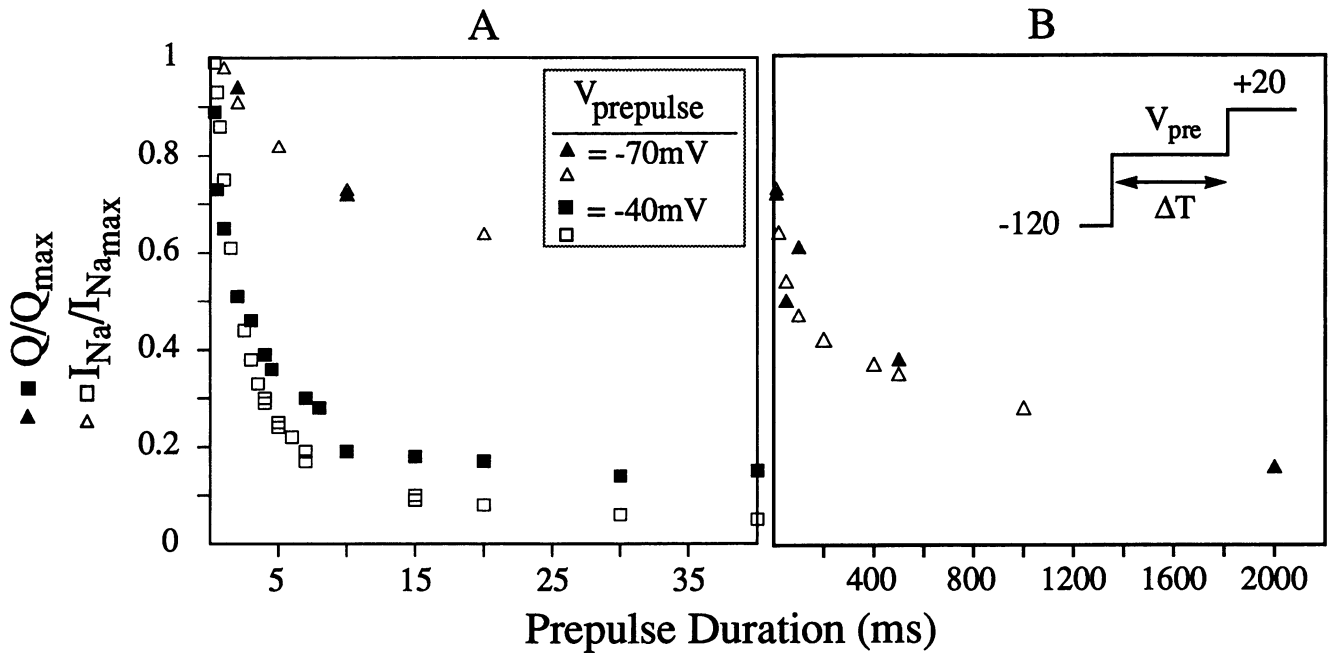
FIGURE 6 Suppression of peak ionic current and suppression of $Q$ON develop with similar kinetics; note the two different time bases used. (*A*) Prepulse durations up to 40 ms. (*B*) Prepulse durations up to 2 s. Ionic currents (*open symbols*) and gating charge (*solid symbols*) were normalized to control currents from a single voltage step to +20 mV. Data at −70 mV (*triangles*) from axon 900416 for both ionic and gating current. Data at −40 mV (*squares*) from axon 900501 for both ionic and gating current. 0//50 Na for ionic currents. 200//0 TMA for gating currents.
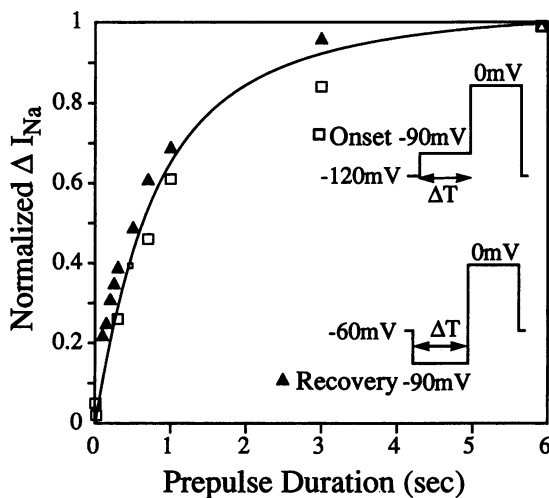


FIGURE 7 Onset (*open squares*) and recovery (*solid triangles*) from slow inactivation have similar rates at the same prepulse voltage. Current amplitudes were normalized to the peak current amplitude following a 6-s prepulse. Onset values were inverted (1 − normalized value) to overlie recovery data. The curve was fitted as a double exponential with a fast time constant of 600 ms and a slow time constant of 2 s. Data from axon 900412. 0//20 Na.

example, at 50 ms, $Q_{ON}$ has recovered by 55% whereas $I_{Na}$ has only recovered by 15%. This difference in recovery between $I_{Na}$ and $Q_{ON}$ diminishes with increasing prepulse durations. By 300 ms, $Q_{ON}$ has recovered by 80% and $I_{Na}$ has recovered by 65%.

Fig. 9 shows the dissociation between the recovery of peak ionic and gating currents in more detail and at two different time bases (*A* in ms and *B* in s). Peak current is significantly slower to recover than charge movement, although the rates become more similar at longer prepulse durations. In addition, Fig. 9 *A* shows that slow inactivation recovery kinetics are apparently sigmoidal because no recovery of $I_{Na}$ is evident in the first 10 ms at the recovery potential of −140 mV. By contrast, the recovery kinetics for charge movement follow an exponential rate. These results suggest that the slow inactivation of ionic current and the slow recovery of gating charge movement are controlled by different processes, separable by their rates of recovery. In addition, these results suggest that recovery of slow inactivation is a multistate process including both faster and slower transitions which account for the initial delay seen in Fig. 9 *A*.

Fig. 9 *B* also demonstrates that recovery is voltage sensitive. Recovery following prolonged depolarization
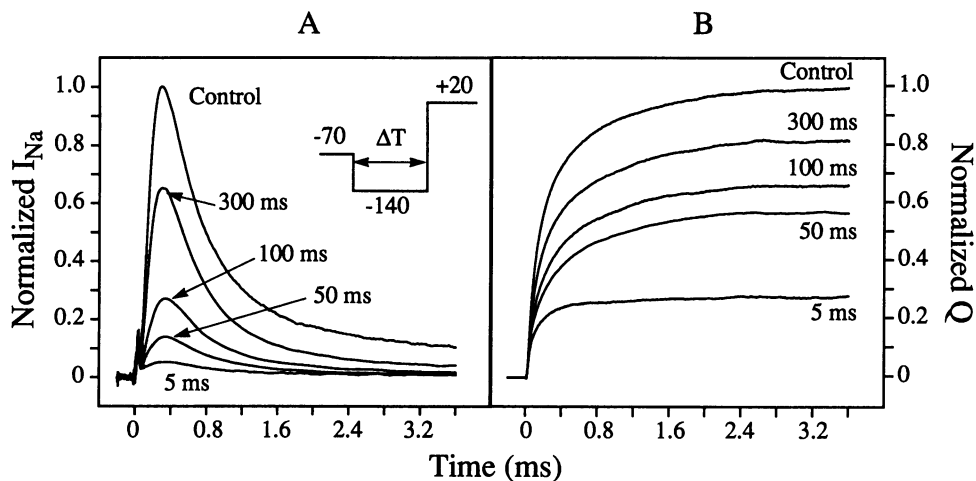
FIGURE 8  Recovery of peak sodium current is slower than recovery of gating charge movement. (*A*) Ionic currents recorded during a depolarizing step to +20 mV after variable times (shown for each current record) at a recovery potential of −140 mV. Currents were normalized to the single pulse to +20 mV (1.4 mA/cm$^2$) from a holding potential of −140 mV. 0//25 Na. Axon 900607. (*B*) Gating charge movement was obtained by integrating gating currents recorded using the same pulse protocols as in *A*. Records were again normalized to the control record (31.2 nC/cm$^2$) from a holding potential of −140 mV to +20 mV. Gating charge can be seen to be relatively larger than the corresponding ionic currents by comparing the records at the same prepulse duration. 0//0 Na, 200 TMA. Axon 900702.

of both ionic current and charge movement is faster when the prepulse potential is −140 mV (*triangles*) than when the prepulse potential is −100 mV (*squares*). However, recovery of gating charge (*solid symbols*) is faster than recovery of slow inactivation (*open symbols*) at both prepulse potentials.

## DISCUSSION

We have presented the following principal observations: (*a*) Change of holding potential equally affects both sodium current and gating charge (Figs. 1 and 4).
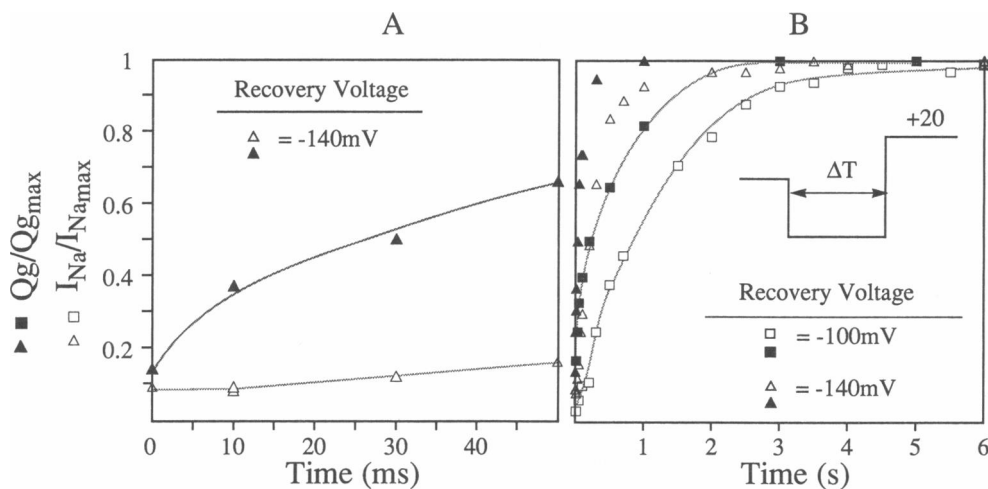


FIGURE 9  Gating charge recovers faster than ionic current recovers from slow inactivation. Shown here are recovery data sets at two different time bases. (*A*) Prepulse durations to 50 ms. (*B*) Prepulse durations to 6 s. In all cases, ionic current can be seen to recover more slowly than gating charge. In addition, the beginning of recovery from slow inactivation appears to be delayed with respect to recovery of gating charge movement (*A*). Data normalized to control single pulse amplitudes. For clarity, lines were fit to matching ionic and gating current sets for recovery voltages of −140 mV (*A*) and −100 mV (*B*). Ionic current from axon 900611. Gating current from axon 900702.

(b) Depolarizing prepulses also affect sodium current and gating charge to similar extents. Slow inactivation of $I_{Na}$ develops with similar kinetics to the suppression of gating charge movement. (c) By contrast, hyperpolarizing prepulses from depolarized $V_h$ do not have similar effects on $I_{Na}$ and gating charge. Recovery of gating charge movement is faster than recovery of $I_{Na}$ from slow inactivation. Ionic current and gating charge can thus be dissociated during recovery. (d) The $h_\infty$ curve shows only one slope with short, <10 ms prepulses. By contrast, an additional slope appears following prepulses with durations of 10 ms or greater as well as in both the $F(V_h)$ and $Q(V_h)$ curves.

## Slow inactivation is an independently voltage-sensitive process

Slow inactivation has been described as a separate and voltage-sensitive process occurring in parallel with both fast inactivation and channel activation (Adelman and Palti, 1969; Starkus and Shrager, 1978). However, a later and more detailed analysis suggested a model involving two separate pathways into the slow inactivated state: (a) a direct path from the open state and, (b) a slower indirect path via the fast inactivated state (Rudy, 1981). This latter model permits the alternative interpretation that slow inactivation is an "absorbing state" which is effectively sequential to channel activation.

The slopes seen for the $Q(V_h)$ data reported by Rayner and Starkus (1989) appeared to fit a single ($\sim 2e$) Boltzmann distribution throughout the range of holding potentials examined. However, the more detailed results obtained in the present study show that the $Q(V_h)$ curve follows the $F(V_h)$ curve in showing both low slope and high slope regions, indicating that channel availability and charge movement are effectively linked when test depolarizations are evoked following sufficiently long equilibration times. The increased slope of the high slope region implies an additional valence that appears only at relatively long prepulse durations (>10 ms) and at voltages more positive than about −90 mV. Hence, the additional valence presumably arises from a voltage sensor that moves too slowly to contribute to gating currents observed within a $\sim$2-ms integration window. We shall argue that this additional slow voltage sensor affects both the $Q(V_h)$ and $F(V_h)$ distributions through electrostatic coupling to the activation mechanism. Thus, the strongly-absorbing slow inactivated state modifies the equilibrium distribution of the activation gating charges.

In contrast to the demonstrable linkage between ionic and gating currents noted above, Bezanilla et al. (1982) and Rayner and Starkus (1989) have reported that gating current recovers more rapidly from long term

inactivation than does $I_{Na}$. Those observations have been repeated here (Figs. 8 and 9), confirming that ionic and gating currents can be uncoupled under appropriately chosen experimental conditions. Although Meves and Vogel (1977) reported that slow recovery of ionic current and gating charge are concurrent in squid axons, they studied recovery between 80 s and 5 min. At these very long times, squid $I_{Na}$ and Ig recovered at apparently equivalent rates. The dissociation between $I_{Na}$ and Ig reported by Bezanilla et al. (1982), also in squid axons, as well as in crayfish axons by Rayner and Starkus (1989) and in this paper, is most prominent within the first 5 ms and thus reflects a different phenomenon from the late recovery studied by Meves and Vogel.

Thus, our evidence suggests that ionic current and gating charge appear associated or dissociated, depending upon the experimental conditions under which they are compared. The apparent conflict can be resolved by the hypothesis that slow inactivation is controlled by an independent voltage sensor within a coupled model (to be presented below). The dissociation between Ig and $I_{Na}$ during recovery further suggests that the hypothesized slow voltage sensor closes channels directly by a "slow inactivation gate," rather than acting indirectly through effects on activation gating.

## Contribution of fast inactivation to steady-state channel availability

Heggeness and Starkus (1986) noted that removal of fast inactivation with $n$-bromoacetamide (NBA) right-shifted both the $F(V_h)$ and $Q(V_h)$ distributions by $\sim$10 mV. (For comparison, in crayfish axons the difference between the midpoints of the $h_\infty$ and $F(V_h)$ curves is $\sim$35 to 40 mV, see Fig. 5.) Additionally, NBA removed the left shifting of the $Q(V_h)$ curve produced by TTX. They reasoned that the TTX effect was mediated by interaction with fast inactivation and that fast inactivation contributed to the total steady-state inactivation which limits channel availability at holding potential. Bezanilla et al. (1982) had similarly concluded that the steady-state gating charge distribution is affected by both fast and slow inactivation processes (although both processes were modeled as voltage-insensitive in that study). Rayner and Starkus (1989) extended this model to crayfish axons, again demonstrating that both fast and slow inactivation are required to match the approach to steady state. However, a higher "coupling energy" was required between activation and slow inactivation to model the greater left-shifting between $Q(V_h)$ and $Q(V)$ curves in crayfish (as opposed to squid) giant axons. We conclude that, although both fast and slow inactivation contribute to steady-state channel availability in crayfish axons, the effect of fast inactivation is relatively small

compared to that of slow inactivation. Furthermore, because the increased slope appearing in the $Q(V_h)$ and $F(V_h)$ curves develops only for prepulse durations $> 10$ ms, we presume that this added valence is associated with slow (rather than fast) inactivation mechanisms. The simple models presented below therefore concentrate on the probable mechanisms of interaction between activation and slow inactivation.

Recent studies of macroscopic inactivation in squid axons (Stimers et al., 1985; Keynes, 1991) also indicate some independent voltage-sensitivity for fast inactivation, although the fast inactivation process appears primarily sequential to prior channel activation. We find that the slope of the $h_\infty$ curve obtained using 2 ms depolarizing pulses from $-120$ mV holding potential (Fig. 5) is not statistically distinguishable from either the slopes of the $F(V)$ curves (see Fig. 3 of Ruben et al., 1990) or the slope of the $Q(V)$ curve seen from a similar holding potential (see Fig. 6 of Rayner and Starkus, 1989). Additionally, we find no change in the apparent valence of the $F(V)$ curve in pronased axons (cf Fig. 4 of Ruben et al., 1990; see also Gonoi and Hille, 1987). The data presented here thus provides no further evidence indicating additional valence associated with fast inactivation in crayfish axons. However, this is hardly surprising. Where fast inactivation is essentially complete within 2 ms, as in crayfish axons, movements of a fast inactivation voltage sensor would occur within the 2-ms gating current integration period used in these studies, and therefore would be included within our observed $Q(V)$ distributions.

## Simulations of experimental data

Our aim in the present study has been to further delineate the physical mechanisms underlying slow inactivation gating. Noting the steeper slope present in the $Q(V_h)$ and $F(V_h)$ distributions but not in their $Q(V)$ and $F(V)$ counterparts, we reasoned that some form of direct interaction must occur between the voltage sensors for activation and slow inactivation. We have tested three major classes of Markovian models that seem reasonably compatible with available structural evidence. Finally, following the lead provided by Zimmerberg et al. (1990) and Goldman (1991), we have reduced these models to their simplest possible form to clarify the behavior of different model classes. These models thus omit the contribution of fast inactivation to steady-state channel availability and represent the complex kinetics of both activation and slow inactivation as simple first order processes. All models presented here assume that closed-to-open transitions are at least 10-fold faster than transitions into the slow inactivated state.

## Sequential models

Scheme I presumes that activation and slow inactivation are tightly coupled by some unspecified allosteric mechanism. Sequential models have received much attention in efforts to model sodium channel activation, particularly in the light of patch-clamp data. However, this formulation falls short of replicating the data we have presented here. Simulations using this model force ionic current and gating

$$C \rightleftharpoons O \rightleftharpoons S$$
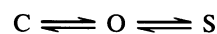
SCHEME I

charge to be associated in steady-state. Thus, recovery fails to show the characteristic dissociation noted in our data (Figs. 8 and 9). The transition from C to O represents activation and determines the shape and position of the $Q(V)$ and $F(V)$ curves. The next transition from O to S generates both slow inactivation of ionic current and, necessarily, a "slow immobilization" of gating current. This transition is a principal determinant of the shape and position of the $Q(V_h)$ and $F(V_h)$ curves. Because return from state S to state C must occur for both $I_{Na}$ and Ig recovery, the sequential model locks together the recovery of gating charge movement and ionic current. Thus, sequential models can not adequately explain the results we have presented.

## Parallel models

Despite the apparent association of gating and ionic currents in steady-state conditions, their dissociation during recovery from prolonged depolarization suggested that slow inactivation might be a separate slow gating process operating in parallel with sodium channel activation. Scheme II presents such a model in simplified form. The simple parallel nature of this model is expressed by the identical kinetics of the 1,2 and 4,3 reactions (shown as vertical in Scheme II) and by the distinct but also identical rates of the 1,4 and 2,3 transitions (horizontal in Scheme II).

However, because of the entirely independent nature
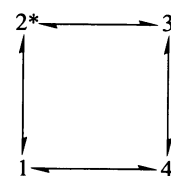


SCHEME II

of the activation and slow inactivation particles in this model, gating charge and ionic current remain dissoci-

ated in steady-state as well as during both depolarizing and hyperpolarizing prepulses. The transition from state 1 to 2* represents activation and determines the $F(V)$ curve; however, the $Q(V)$ and $Q(V_h)$ curves are determined jointly by the 1,2 and 4,3 transitions. The 1,4 and 2,3 transitions represent slow inactivation and determine the $F(V_h)$ curve. Thus, the $Q(V_h)$ and $F(V_h)$ distributions are independent under all conditions. The behavior of this model is thus inconsistent with our experimental observations, in which we see that gating charge and ionic current are coupled in steady state and during depolarizing prepulses, yet dissociate during recovery from depolarized holding potentials. Thus, strictly parallel models are also inadequate to explain our experimental results.

## Coupled-parallel models

We have obtained markedly more successful results using a modified version of the four-state model introduced by Bezanilla et al. (1982) and further studied by Fernandez et al. (1982). Within this model, activation and slow inactivation were presumed to be parallel, cooperatively coupled processes. The principal addition made here has been to add independent voltage-sensitivity to the slow inactivation mechanism.

Interactions between voltage sensors were simulated using both anti-cooperative (repulsion) and cooperative (attraction) interactions to couple the activation voltage sensor with the voltage sensor controlling slow inactivation. We have not been able to achieve satisfactory results from any models based on the anticooperative approach. Hence, a cooperatively coupled model, shown in Scheme III, was tested for its ability to simulate the major observations presented here. Position 1 represents the closed state. Position 2* represents the open state, and positions 4 and 3 represent comparable slow inactivated states.

Cooperative coupling between activation and slow



SCHEME III
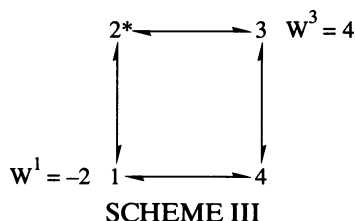
inactivation is specified as a change in well energy ($W_a$ or $W_b$) following the approach introduced by Bezanilla, et al. (1982). Thus, the attraction between the activation and inactivation particles effectively increases well-to-barrier height. All models specified in this manner

necessarily comply with requirements of microscopic reversibility, despite the symmetry or asymmetry of the coupling energies. In accordance with the physical model described below, such coupling occurs for those states in which both particles are in their hyperpolarized- or depolarized-favored positions (i.e., states 1 and 3 in Scheme III). Well-to-barrier heights are specified for the hyperpolarization-favored ($\omega a$) and depolarization-favored ($\omega b$) energy wells in kT units, and valences ($z$) and barrier positions ($d$) are as shown in Table 3 for each set of transitions. Reaction rates were calculated using the modified rate equations introduced by Bezanilla et al., (1982). Thus, where $K_\alpha$ is the rate constant of the depolarization-favored transition and $K_\beta$ is the hyperpolarization-favored back reaction rate, then:

$$K_\alpha = (kT/h) \cdot \exp([W_a - \omega_a + ezd\,V]/kT)$$
$$K_\beta = (kT/h) \cdot \exp([W_b - \omega_b - ez(1 - d)V]/kT),$$

where $e$ is the electronic charge, $V$ is the membrane potential, $k$ is the Boltzmann constant, $h$ is the Planck constant, and $T$ is the absolute temperature. We here consider the particle that makes transitions between states 1 and 2, or 4 and 3 to be the voltage sensor responsible for channel activation. For simplicity, we have limited the present model to a single activation particle with only two stable positions: a hyperpolarization-favored state in which the channel is closed; and a depolarization-favored state in which the channel is open unless slow inactivated. The particle which moves between states 2 and 3, or 1 and 4 is the voltage sensor that controls slow inactivation. See Methods for further description of modeling procedures.

Simulations run using this simplified model produce data that correspond with all of the major observations reported in this paper. Fig. 10 shows that the voltage dependence of the $F(V_h)$ and $Q(V_h)$ curves generated by this model are similar to those we derived from our experiments on crayfish axons. Furthermore, the high slope region of the $F(V_h)$ and $Q(V_h)$ curves only develops when the slow inactivation reactions (between states 2 to 3 and 1 to 4) are given independent voltage sensitivity. Finally, Fig. 11 shows (at a short time scale in Fig. 11 A and a long time scale in Fig. 11 B) that

TABLE 3 Simulation parameters

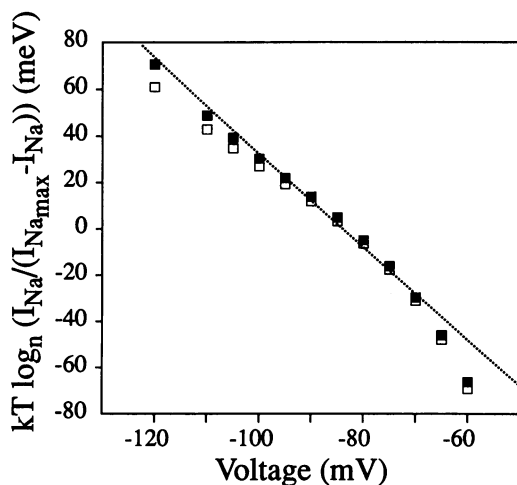| Transition | $W_a$ | $\omega a$ | $W_b$ | $\omega b$ | $z$ | $d$ | $V_0$ |
|---|---|---|---|---|---|---|---|
| 1,2 | −2 | 19 | 0 | 24.5 | 1.8 | 0.5 | −46.86 |
| 4,3 | 0 | 19 | −4 | 24.5 | 1.8 | 0.5 | −127.19 |
| 1,4 | −2 | 26.3 | 0 | 32.4 | 1.5 | 0.5 | −65.87 |
| 2,3 | 0 | 26.3 | −4 | 32.4 | 1.5 | 0.5 | −162.27 |

FIGURE 10  Simulated $Q(V_h)$ and $F(V_h)$ data. Logit-transformed simulated data shows close correspondence in steady-state voltage dependence between peak sodium current (*open squares*) and gating charge movement (*solid squares*). Simulated data midpoint = −85 mV, low slope = 1.9*e*, high slope = 3.7*e*. Dashed line is a 2*e* Boltzmann distribution with a midpoint of −85 mV.

recovery of simulated gating charge movement (*solid symbols*) is faster than recovery of simulated ionic current from slow inactivation (*open symbols*) and, just as in our data (Fig. 9*A*), initial recovery of $I_{Na}$ shows sigmoidal kinetics.

The Scheme III model shown here has much in common with the activation/inactivation models explored by Bezanilla et al. (1982), Brum and Rios (1987), and Rayner and Starkus (1989). These models distinguish the gating currents of normal channel activation (charge 1 of Brum and Rios; simulated in Scheme III by the 1,2 reaction) from the movements of inactivated
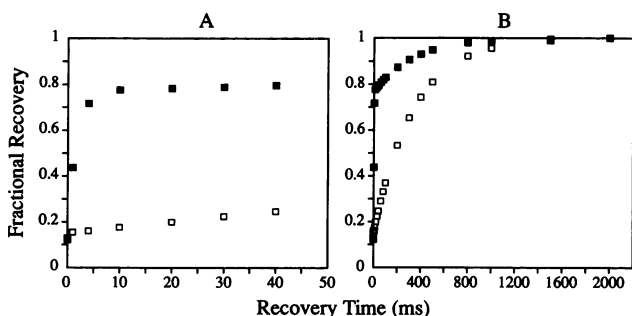


FIGURE 11  Simulated data showing dissociation between recovery of gating charge movement (*solid squares*) and peak ionic current (*open squares*) at two different time bases for comparison with the experimental results shown in Fig. 9. Holding potential was −65 mV and recovery potential was −140 mV.

gating charge (charge 2 of Brum and Rios; simulated here by the 4,3 reaction). Thus the Q(V) curve for the Scheme III model is determined entirely by the 1,2 reaction, whereas the $Q(V_h)$ curve represents the equilibrium distribution between the 1,2 and 3,4 charge movements (i.e. between charge 1 and charge 2 in the terminology of Brum and Rios, 1987). However, the fast charge movements of these transitions must be accompanied by very slow movements of these same gating charges, resulting from the slow processes of equilibration between the 1,2 and 4,3 pathways (as pointed out by Rayner and Starkus, 1989). We here add the additional concept that the slow inactivation mechanism (which shifts charges from the 1,2 to the 4,3 pathway) is itself voltage sensitive and must therefore be expected to generate an additional, theoretically-detectable, component of gating current. In practice, such currents would be difficult to measure by direct methods due to their very slow rates of equilibration ( ~ 100-fold slower than for activation gating charge movements). Nevertheless, it may not be immediately obvious how the very simple Scheme III model separates recovery of gating current from recovery of ionic current after prolonged depolarization: At depolarized holding potentials, channels accumulate in state 3; however, following a recovery pulse to a hyperpolarized potential, channels move rapidly to state 4 but slowly thereafter to state 1 (by the slow 4,1 transition); following a subsequent depolarizing test pulse from the recovery potential, only the few channels that have recovered as far as state 1 can reach the open state (2*) thereby generating both gating and ionic current, whereas the more numerous channels moving from state 4 back to state 3 generate gating current but no ionic current. By contrast, during depolarizing prepulses, ionic current and gating charge movement are necessarily coupled because both are associated with the pathway from state 1, through 2*, to state 3 (involving the voltage-sensitive slow inactivation reaction).

The four-state kinetic model described above differs from the four-state kinetic scheme used by Bezanilla et al. (1982) and Fernandez et al. (1982) principally by ascribing independent voltage-sensitivity to the slow inactivation reaction. However, an important additional contribution of those earlier models was that they suggested physical mechanisms that might underlie the observed kinetic phenomena; a negatively-charged activation particle was presumed to interact with an externally-located and positively-charged slow inactivation gate. Their model can be brought into line with more recent evidence (summarized below) indicating that the primary voltage sensors of the sodium channel are its positively-charged S4 segments, by presuming the S4 segments controlling channel activation interact with an

internally-located and negatively-charged slow inactivation gate. Our contribution here is to suggest that this slow inactivation gate moves in the applied transmembrane voltage field, carrying an equivalent charge of at least $1.5e$.

## Structural implications of voltage-sensitive slow inactivation

Much attention has been directed at elucidating structure-function relationships within the sodium channel molecule, with most effort being focused on the parts of the protein that control activation. Stühmer et al. (1989) have elegantly shown that deletion and replacement mutations of charged residues in the S4 segments of Domain I has profound effects on the kinetics and voltage sensitivity of sodium channel activation. On the other hand, conservative mutations in Domain II also affect activation and fast inactivation properties (Auld et al., 1990). Although the parts of the sodium channel that control fast inactivation remain uncertain, there is strong evidence that an $NH_2$-terminus "ball and chain" controls inactivation in A-type potassium channels (Hoshi et al., 1990; Zagotta et al., 1990). In sodium channels, antibodies to a peptide sequence in the linker between domains III and IV modify the kinetics of inactivation without affecting activation (Vassilev et al., 1988). However, point mutations resulting in neutralization or sign reversal in the III-IV linker increased, rather than decreased, the rate of inactivation and slowed activation kinetics (Moorman et al., 1990). Thus, the structure/function relationships underlying fast inactivation remain equivocal in sodium channels.

By contrast, little structural information relating to slow inactivation is available. Preliminary evidence suggests that the carboxy-terminus might be involved with slow inactivation of the A-type potassium channel (Zagotta et al., 1991). However, slow inactivation in those channels does not appear to be voltage sensitive, as opposed to the results we have presented here, suggesting a molecular mechanism very different to that operating in Na channels. The data presented here indicate that slow inactivation is controlled by its own voltage sensor. Apparently some part of the channel molecule responds very slowly to changes in voltage but then initiates a separate gating mechanism which closes sodium channels (and holds them in a nonconducting state despite activation of the fast gating particles). Because the additional valence added by this slow process is similar to the apparent valence of activation (Ruben et al., 1990), one possibility deserving further consideration is that slow inactivation might be controlled by one of the S4 segments.

## REFERENCES

Adelman, W. J., and Y. Palti. 1969. The effects of external potassium and long duration voltage conditioning on the amplitude of sodium currents in the giant axon of the squid, *Loligo peali. J. Gen. Physiol.* 54:589–606.

Alicata, D. A., M. D. Rayner, and J. G. Starkus. 1989. Osmotic and pharmacological effects of crayfish giant axons. *Biophys. J.* 55:347–353.

Armstrong, C. M., and F. Bezanilla. 1977. Inactivation of the sodium channel. II. Gating current experiments. *J. Gen. Physiol.* 70:567–590.

Auld, V. J., A. L. Goldin, D. S. Krafte, W. A. Catterall, H. A. Lester, N. Davidson, and R. J Dunn. 1990. A neutral amino acid change in segment II S4 dramatically alters the gating properties of the voltage-dependent sodium channel. *Proc. Natl. Acad. Sci. USA.* 87:323–327.

Bezanilla, F., and C. M. Armstrong. 1977. Inactivation of the sodium channel. I. Sodium current experiments. *J. Gen. Physiol.* 70:549–566.

Bezanilla, F., R. E. Taylor, and J. M. Fernandez. 1982. Distribution and kinetics of membrane dielectric polarization. I. Long-term inactivation of gating currents. *J. Gen. Physiol.* 79:21–40.

Brismar, T. 1977. Slow mechanism for sodium permeability inactivation in myelinated nerve fibre of *Xenopus laevis. J. Physiol. (Lond.).* 270:283–297.

Brum, G., and E. Rios. 1987. Intramembrane charge movement in frog skeletal muscle fibres. Properties of charge 2. *J. Physiol. (Lond.).* 387:489–517.

Chandler, W. K., and H. Meves. 1970a. Sodium and potassium currents in squid axons perfused with fluoride solutions. *J. Physiol. (Lond.).* 211:623–652.

Chandler, W. K., and H. Meves. 1970b. Evidence for two types of sodium conductance in axons perfused with sodium fluoride solution. *J. Physiol. (Lond.).* 211:653–678.

Chandler, W. K., and H. Meves. 1970c. Rate constants associates with changes in sodium conductance in axons perfused with sodium fluoride. *J. Physiol. (Lond.).* 211:679–705.

Chandler, W. K., and H. Meves. 1970d. Slow changes in membrane permeability and long lasting action potentials in axons perfused with fluoride solutions. *J. Physiol. (Lond.).* 211:707–728.

Fernandez, J. M., F. Bezanilla, and R. E. Taylor. 1982. Distribution and kinetics of membrane dielectric polarization. II. Frequency domain studies of gating currents. *J. Gen. Physiol.* 79:41–67.

Glasstone, S., K. J. Laidler, and H. Eyring. 1941. The Theory of Rate Processes. McGraw-Hill Inc., New York. 522–599.

Goldman L. 1991. Gating current kinetics in *Myxicola* giant axons: order of the back transition rate constants. *Biophys. J.* 59:574–589.

Gonoi, T. and B. Hille. 1987. Gating of Na channels. Inactivation modifiers discriminate among models. *J. Gen. Physiol.* 89:253–274.

Heggeness, S. T., and J. G. Starkus. 1986. Saxitoxin and Tetrodotoxin. Electrostatic effects on sodium channel gating current in crayfish giant axons. *Biophys. J.* 49:629–643.

Hodgkin, A. L., and A. F. Huxley. 1952. A quantitative description of membrane current and its application to conduction and excitation in nerve. *J. Physiol. (Lond.).* 117:500–544.

Hoshi, T., W. N. Zagotta, and R. W. Aldrich. Biophysical and molecular mechanisms of *Shaker* Potassium channel inactivation. *Science (Wash., DC).* 250:533–538.

Keynes, R. D. 1991. On the voltage dependence of inactivation in the sodium channel of the squid giant axon. *Proc. R. Soc. Lond. B Biol. Sci.* 243:47–53.

Meves, H., and W. Vogel. 1977. Slow recovery of sodium current and 'gating current' from inactivation. *J. Physiol. (Lond.).* 267:395–410.

Moorman, J. R., G. E. Kirsch, A. M. J. Van Dongen, R. H. Joho, and A. M. Brown. 1990. Fast and slow gating of sodium channels encoded by a single mRNA. *Neuron.* 4:243–252.

Narahashi, T. 1964. Restoration of action potential by anodal polarization in lobster giant axons. *J. Cell. Comp. Physiol.* 64:73–96.

Oxford, G., and J. Z. Yeh. 1985. Interactions of monovalent cations with sodium channels in squid axon. I. Modification of physiological inactivation gating. *J. Gen. Physiol.* 85:583–602.

Quandt, F. N. 1987. Burst kinetics of sodium channels which lack fast inactivation in mouse neuroblastoma cells. *J. Physiol. (Lond.).* 392:563–585.

Rayner, M. D., and J. G. Starkus. 1989. The steady-state distribution of gating charge in crayfish giant axons. *Biophys. J.* 55:1–19.

Ruben, P. C., J. G. Starkus, and M. D. Rayner. 1990. Holding potential affects the apparent voltage-sensitivity of sodium channel activation in crayfish giant axons. *Biophys. J.* 58:1169–1181.

Ruben, P. C., and J. G. Starkus. 1991. Parallel and sequential processes in slow inactivation of sodium channels. *Biophys. J.* 59:71a. (Abstr.)

Rudy, B. 1978. Slow inactivation of the sodium conductance in squid giant axons. Pronase resistance. *J. Physiol. (Lond.).* 283:1–21.

Rudy, B. 1981. Inactivation in *Myxicola* giant axons responsible for slow and accumulative adaptation phenomenon. *J. Physiol. (Lond.).* 283:1–21.

Ruff, R., L. Simoncini, and W. Stühmer. 1987. Comparison between slow sodium channel inactivation in rat slow- and fast-twitch muscle. *J. Physiol. (Lond.).* 383:339–348.

Schauf, C. L., T. L. Peneck, and F. A. Davis. 1976. Slow inactivation in *Myxicola* axons. *Biophys. J.* 16:771–778.

Shrager, P. 1974. Ionic conductance changes in voltage clamped crayfish axons at low pH. *J. Gen. Physiol.* 64:666–690.

Simoncini, L., and W. Stühmer. 1987. Slow sodium channel inactivation in rat fast-twitch muscle. *J. Physiol. (Lond.).* 383:327–337.

Starkus, J. G., and M. D. Rayner. 1991. Gating current "fractionation" in crayfish giant axons. *Biophys. J.* 60:1101–1119.

Starkus, J. G. and P. Shrager. 1978. Modification of slow sodium inactivation in nerve after internal perfusion with trypsin. *Am. J. Physiol.* 4:C238–244.

Stimers, J. R., F. Bezanilla and R. E. Taylor. 1985. Sodium channel activation in the squid giant axon. steady-state properties. *J. Gen. Physiol.* 85:65–82.

Stühmer, W., F. Conti, H. Suzuki, X. Wang, M. Noda, N. Yahagi, H. Kubo, and S. Numa. 1989. Structural parts involved in activation and inactivation of the sodium channel. *Nature (Lond.).* 339:597–603.

Vassilev, P. M., T. Scheuer, W. A. Catterall. 1988. Identification of an intracellular peptide segment involved in sodium channel inactivation. *Science (Wash., DC).* 24:1658–1661.

Woodbury, J. W. 1971. Eyring rate theory model of the current-voltage relationships of ion channels in excitable membranes. *In* Chemical Dynamics: Papers in Honor of Henry Eyring. J. O. Hirschfelder, editor. John Wiley & Sons, Inc., New York. 601–617.

Zagotta, W. N., T. Hoshi, and R. W. Aldrich. 1990. Restoration of inactivation in Mutants of *Shaker* potassium channels by a peptide derived from ShB. *Science (Wash., DC).* 250:568–571.

Zagotta, W. N., T. Hoshi, and R. W. Aldrich. 1991. Molecular separation of two inactivation processes in *Shaker* potassium channels. *Biophys. J.* 59:3a. (Abstr.)

Zimmerberg, J., F. Bezanilla, and V. A. Parsegian. 1990. Solute inaccessible aqueous volume changes during opening of the potassium channel of the squid giant axon. *Biophys. J.* 57:1049–1064.